

The core starbursts of the galaxy NGC 3628: Radio very long baseline interferometry and X-ray studies

XIAOLONG YANG (杨小龙) ^{1,2} AND ZIWEI OU (区子维) ³

¹*Shanghai Astronomical Observatory, Chinese Academy of Sciences, Shanghai 200030, China*

²*Shanghai Key Laboratory of Space Navigation and Positioning Techniques, Shanghai 200030, China*

³*School of Physics and Astronomy, Sun Yat-sen University, Zhuhai 519082, China*

(Received XXX; Revised XXX; Accepted XXX)

Submitted to ApJ

ABSTRACT

We present radio very long baseline interferometry (VLBI) and X-ray studies of the starburst galaxy NGC 3628. The VLBI observation at 1.5 GHz reveals seven compact (0.7–7 parsec) radio sources in the central ~ 250 parsec region of NGC 3628. Based on their morphology, high radio brightness temperatures ($10^5 - 10^7$ K), and steep radio spectra, none of these seven sources can be associated with active galactic nuclei (AGNs); instead, they can be identified as supernova remnants (SNRs), with three of them appearing consistent with partial shells. Notably, one of them (W2) is likely a nascent radio supernova and appears to be consistent with the star formation rate of NGC 3628 when assuming a canonical initial mass function. The VLBI observation provides the first precise measurement of the diameter of the radio sources in NGC 3628, which allow us to fit a well-constrained radio surface brightness - diameter ($\Sigma - D$) correlation by including the detected SNRs. Furthermore, future VLBI observations can be conducted to measure the expansion velocity of the detected SNRs. In addition to our radio VLBI study, we analyze *Chandra* and *XMM-Newton* spectra of NGC 3628. The spectral fitting indicates that the SNR activities could well account for the observed X-ray emissions. Along with the *Chandra* X-ray image, it further reveals that the X-ray emission is likely maintained by the galactic-scale outflow triggered by SN activities. These results provide strong evidence that SN-triggered activities play a critical role in generating both radio and X-ray emissions in NGC 3628 and further suggest that NGC 3628 is in an early stage of starbursts.

Keywords: Starburst galaxies (1570) — Supernova remnants (1667) — Very long baseline interferometry (1769) — Radio sources (1358) — X-ray sources (1822)

1. INTRODUCTION

Galaxies with enhanced star formation compared with normal spiral galaxies, especially in the central nuclear region, are known as starburst galaxies (Lehnert & Heckman 1996). They have star formation rates (SFRs) several to hundreds of times higher than ordinary galaxies like the Milky Way. Studying nearby starburst galaxies may shed light on our understanding of the evolution

of their high redshift cousin in the early Universe (e.g. Rinaldi et al. 2022).

Starburst is an important episode in galaxy evolution (Hopkins et al. 2006; Zhang et al. 2018); it lasts up to a few hundred million years (e.g. McQuinn et al. 2018). Simulations and observations indicate that the starburst activity can be triggered by mergers or close flybys between two galaxies (Mihos & Hernquist 1996; Schweizer 2005; Di Matteo et al. 2007; Montuori et al. 2010). These interactions push the gas inflow toward the center of galaxies, where it reaches sufficient density to cause large numbers of massive stars to form (Combes 2000). In addition, the birth (stellar feedback) and death (supernova explosion) of massive stars can

generate shocks to compress the gas and further enhance the star formation (McCray & Kafatos 1987; Shetty & Ostriker 2008; Fall et al. 2010; Skinner & Ostriker 2015). However, the interplay between a galactic scale outflow and the gas inflow and compression will regulate, slow down and eventually brake the intense star-forming process (Chevalier & Clegg 1985; Tomisaka & Ikeuchi 1988; Heckman et al. 1990; Cooper et al. 2008).

Star-forming galaxies typically host rich populations of ultradense (UD) H II regions (Kobulnicky & Johnson 1999; Johnson et al. 2001) where massive stars are born. On the other hand, the large population of massive stars will rapidly evolve and end their lifetime with supernova explosions (supernovae, SNe) and form supernova remnants (SNRs) (Engelbracht et al. 1998). These UD H II regions are probes of recent star formation, while SNe and SNRs are vital tracers of star formation history and are responsible for the galactic scale feedback. The central regions of the majority of starbursts are obscured optically. However, radio emissions, which are unaffected by extinction, allow the central regions of these galaxies to be probed. The radio emissions include both non-thermal (synchrotron) emission, arising from the acceleration of particles to relativistic speeds in SNe and SNRs, and thermal free-free emission from UD H II regions (Condon 1992). Furthermore, X-ray binaries (XRBs) and active galactic nuclei (AGNs) may also reside in star-forming galaxies, especially, AGNs can produce both thermal (Gallimore et al. 2004; Laor & Behar 2008; Ruginski & Laor 2016; Inoue & Doi 2018; Baskin & Laor 2021; Yang et al. 2022a) and non-thermal (Zakamska & Greene 2014; Nims et al. 2015; Yang et al. 2020, 2022b,c) radio emissions; they may also contribute significant radio emissions in starburst galaxies (e.g. Gallimore et al. 2004; Middelberg et al. 2007).

High-resolution very long baseline interferometry (VLBI) observations can resolve (constrain the size of) individual UD H II region, SN, and SNR in nearby star-forming galaxies. The great success of using VLBI on this subject focuses on several nearby star-forming galaxies, e.g. M82 (Pedlar et al. 1999; Beswick et al. 2006; Fenech et al. 2010), Arp 220 (Rovilos et al. 2005; Lonsdale et al. 2006; Parra et al. 2007; Batejat et al. 2011), Arp 299 (Neff et al. 2004; Ulvestad 2009; Bondi et al. 2012), NGC 253 (Rampadarath et al. 2014) and NGC 4945 (Lenc & Tingay 2009). Observations of these objects may help us to understand the environment of starburst cores (Batejat et al. 2011), since the evolution of SNe and SNRs is regulated by dense interstellar medium (ISM). Furthermore, SNe and SNRs are likely responsible for the origin of the well-known FIR-radio correlation and the galactic scale outflow, and the VLBI

observations of these sources may provide useful inputs for models. Especially, with VLBI monitoring observations, it is possible to track the evolution of individual SN and SNR, and alert nascent SNe (Marcaide et al. 1995, 2009; Varenius et al. 2019). In this work, we will visit the starburst galaxy NGC 3628.

NGC 3628 is a nearby ($D = 10.6$ Mpc or $z = 0.0028$, Gerke et al. 2015), edge-on Sbc galaxy (Carral et al. 1990). The source is also a member of the interacting group the Leo Triplet, together with the other two galaxies NGC 3623 and NGC 3627. NGC 3628 is a sub-LIRG (sub-luminous infrared galaxy, $10^{10}L_{\odot} \leq L_{\text{IR}} < 10^{11}L_{\odot}$) with infrared luminosity $L_{\text{IR}} = 1.7 \pm 0.4 \times 10^{10}L_{\odot}$ (Falstad et al. 2021). In particular, no evidence of an obscured AGN was found in NGC 3628 (Falstad et al. 2021). The high infrared luminosity of NGC 3628 is interpreted as evidence of intense star formation. In addition, NGC 3628 satisfies the well-known FIR-radio correlation for star-forming galaxies, indicating that the central engine is dominated by star formation. NGC 3628 maintains wide-scale outflows, including a sub-kpc scale molecular gas outflow (Irwin & Sofue 1996; Tsai et al. 2012; Cicone et al. 2014; Roy et al. 2016) and kpc-scale ionized gas outflows (Sharp & Bland-Hawthorn 2010; Hermosa Muñoz et al. 2022). Again, X-ray observations with high enough resolution reveal a soft X-ray halo in the central region of NGC 3628 (Strickland et al. 2002, 2004; Tsai et al. 2012), which mimics a warm gas outflow. Through high-resolution radio observations (Carral et al. 1990; Cole et al. 1998, VLA A-array 15 GHz and MERLIN 1.4 GHz, respectively), a list of compact radio sources were identified as star-forming products. Therefore, combining radio and X-ray observations may help to confirm the nature of star forming galaxies (Wik et al. 2014; Pannuti et al. 2015). Unfortunately, previous radio observations were unable to resolve the central radio sources, so a higher resolution is necessary to determine their sizes and structures.

This work present VLBI 1.5 GHz observational studies of the starburst galaxy NGC 3628, and this observation was to search for the potential low luminosity AGN in NGC 3628, probe the nuclear radio sources and constrain their sizes. The archival X-ray data of NGC 3628 are also analyzed to ensure a better understanding of the central engine of the galaxy NGC 3628. In Section 2, we present observation and data reduction. We present the data reduction results in Section 3. In Section 4, we discuss the identification of the radio sources detected by VLBI, the model-fits of X-ray spectra, and the explanation of the X-ray and radio emissions. Finally, in Section 5, we give our conclusions. Throughout this

work, we assume a distance of 10.6 Mpc to NGC 3628, which yields a size scale of $0.051 \text{ pc mas}^{-1}$, and take the standard Λ CDM cosmology with $\Omega_{\Lambda} = 0.71$, $\Omega_m = 0.27$ and $T_{cmb} = 2.732 \text{ K}$.

2. OBSERVATION AND DATA REDUCTION

2.1. VLBA

We observed NGC 3628 on 2021 July 13 with eight VLBA antennas at L -band (1.545 GHz, hereafter using 1.5 GHz for short, the project code BA146). The total observation time is 2 hr with a data recording rate of 2 Gbps. The observation was performed in phase-referencing mode, using J1118+1234 ($\alpha = 11^{\text{h}}18^{\text{m}}57^{\text{s}}.301434$, $\delta = +12^{\circ}34'41''.71798$, J2000, i.e. 1.06° to the target) as the phase reference calibrator. The VLBA data calibration was performed in the Astronomical Image Processing System (AIPS), a software package that was developed by the National Radio Astronomy Observatory (NRAO) of USA (Greisen 2003), following the standard procedure. A priori amplitude calibration was performed using the system temperatures and antenna gain curves provided by each station. The Earth orientation parameters were obtained and calibrated using the measurements from the US Naval Observatory database, and the ionospheric dispersive delays were corrected from a map of the total electron content provided by the Crustal Dynamics Data Information System (CDDIS) of NASA¹. The opacity and parallactic angles were also corrected using the auxiliary files attached to the data. The delay in the visibility phase was solved using the phase reference calibrator J1118+1234. A global fringe-fitting on the phase-referencing calibrator was performed by taking the calibrator’s model to solve miscellaneous phase delays of the target. The calibrated data of the target was then exported to DIFMAP (Shepherd 1997) for self-calibration and model-fit. Especially, we first performed a uv-tapper in DIFMAP by 0.1 at $5M\lambda$ to construct a low-resolution image, where a two-dimensional Gaussian model-fit was used. Only sources with signal-to-noise ratios above 5 were fitted. The middle panel of Figure 1 shows the uv-tapered image of NGC 3628. Next, the full-resolution image of each Gaussian component was established with `clean` in DIFMAP, and we especially consult the positions of components W1 and E2 from the Gaussian models. No self-calibration was applied to the target source due to the low signal-to-noise ratios. The full-resolution images for each source were created using natural weights; see subset images

in Figure 1. Based on a well-established understanding of their nature, a model fit using an optically thin sphere was conducted to determine the sizes and flux densities of these radio sources (see Section 4.2). Furthermore, we obtain VLA B-array 1.4 GHz image from the FIRST survey (the Faint Images of the Radio Sky at Twenty-centimeters, Becker et al. 1995)² and VLA D-array 1.5 GHz (observed on 1988-03-25, the project ID. AS300 and PI: G. Siemieniec) and A-array 4.86 GHz (observed on 1984-12-10, the project ID. AW122 and PI: A.E. Wehrle, Wehrle 1987) images from the NRAO Archive³, see the contours in Figure 2.

We estimate uncertainties in coordinates by accounting for three main origins: (1) Positional uncertainties of phase-referencing calibrators. In phase-referencing observations, the coordinates of the target are referenced by a closed calibrator. The calibrator J1118+1234 was elected from the catalog `rfc_2022a` in `Astrogeo`⁴ with precise position with accuracies $\Delta\alpha = 0.10 \text{ mas}$ in right ascension and $\Delta\delta = 0.10 \text{ mas}$ in declination; (2) Astrometric accuracy of phase-referenced observations. Primarily concerning the station coordinate, Earth orientation, and troposphere parameter uncertainties, which can be measured through the formula and parameters from Pradel et al. (2006). This portion contributes position errors: $\Delta\alpha \approx 0.26 \text{ mas}$ and $\Delta\delta \approx 0.50 \text{ mas}$ in this VLBA 1.5 GHz observation; (3) Thermal error due to the random noise (e.g. Rioja et al. 2017). This uncertainty can be characterized as $\sigma_t \sim \theta_B / (2 \times \sigma_{SNR})$, where θ_B is the full-width at half maximum of the restoring beam and σ_{SNR} is the signal-to-noise ratio. In this work, we measure the thermal error via a Gaussian model-fit in DIFMAP. In Table 1, we list the coordinates along with the estimated uncertainties of the coordinates for each VLBI source.

We estimate flux density uncertainties following the instructions described by Fomalont (1999). In this work, the integrated flux densities S_i were extracted from the Gaussian model-fit in DIFMAP with the task `modelfit`, where a standard deviation in the model-fit was estimated for each source and considered as the fitting noise error. Additionally, we assign the standard 5% errors originating from amplitude calibration of VLBA (see VLBA Observational Status Summary 2021A⁵).

² <http://sundog.stsci.edu/>

³ <https://data.nrao.edu/>

⁴ <http://astrogeo.org/>

⁵ <https://science.nrao.edu/facilities/vlba/docs/manuals/oss2021A>

¹ <https://cddis.nasa.gov>

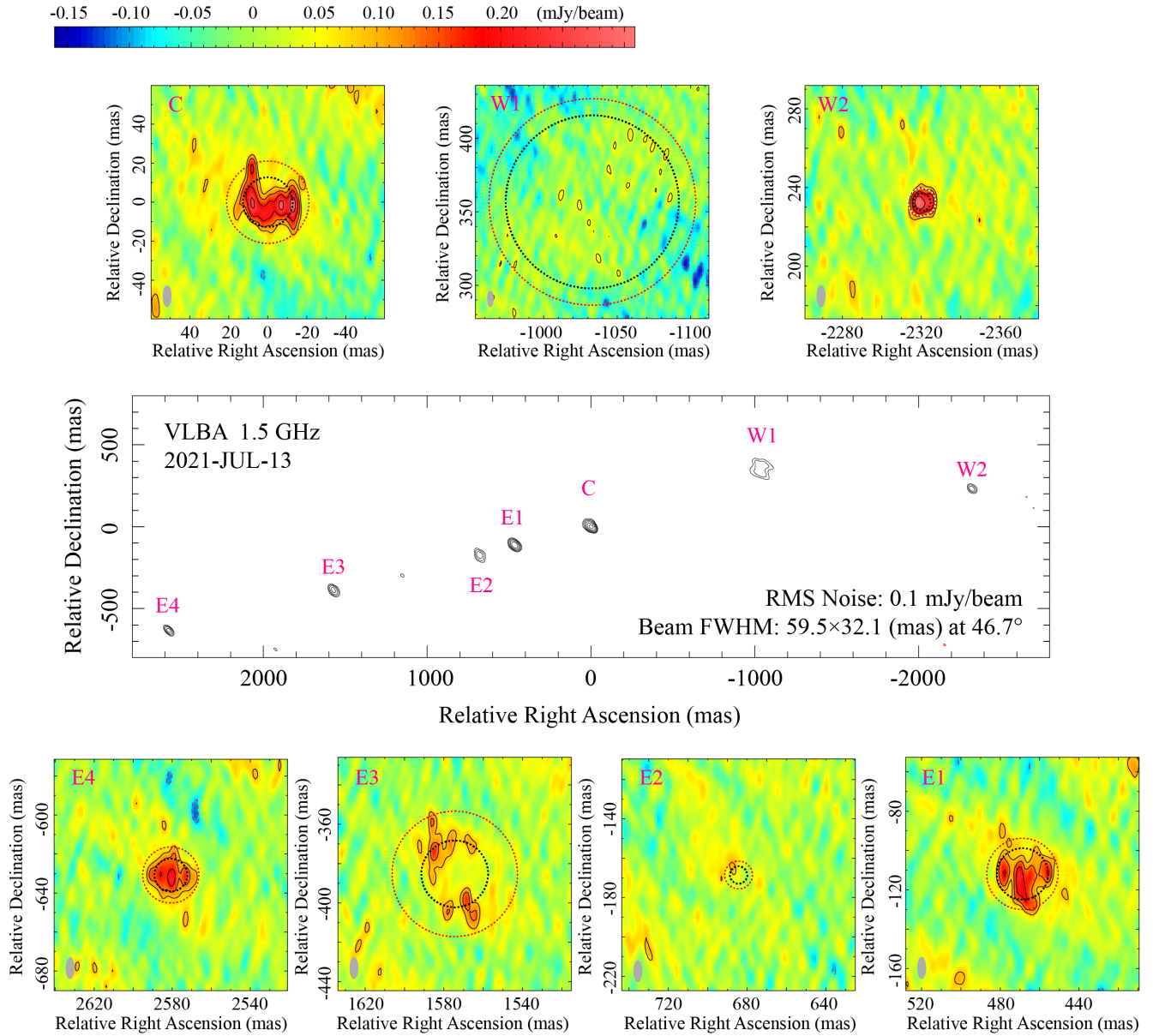


Figure 1. VLBA 1.5 GHz images of NGC 3628. *The middle panel:* the uv-tapered images of NGC 3628; *Upper and lower panels:* the full resolution images of each source presented in the middle panel, where the grey ellipses in the bottom left corner of each panel represent the full width at half-maximum (FWHM) of the restoring beam, they are all the same, i.e. 11.2×4.47 at -0.63° . The contours are at $3\sigma \times (-1, 1, 1.41, 2, 2.83, \dots)$, where 1σ noises are 0.1 and $0.03 \text{ mJy beam}^{-1}$ for the full resolution and uv-tapered contours, respectively. The black and red/white circles in each upper and lower panel indicate the component size obtained via Gaussian and spherical model-fits, respectively.

2.2. X-ray

NGC 3628 was observed by *Chandra* ACIS-S on December 2, 2000 (ObsID: 2039, PI: David K. Strickland; Strickland et al. 2001) with FAINT mode and a total exposure time of 57.96 ks. We retrieved the data from

the *Chandra* data archive, performed data reduction, and constructed the X-ray spectrum with the *Chandra* Interactive Analysis of Observations software package (CIAO, Fruscione et al. 2006)⁶ version 4.13. The data was initially reprocessed according to the *Chandra*

⁶ <https://cxc.cfa.harvard.edu/ciao/>

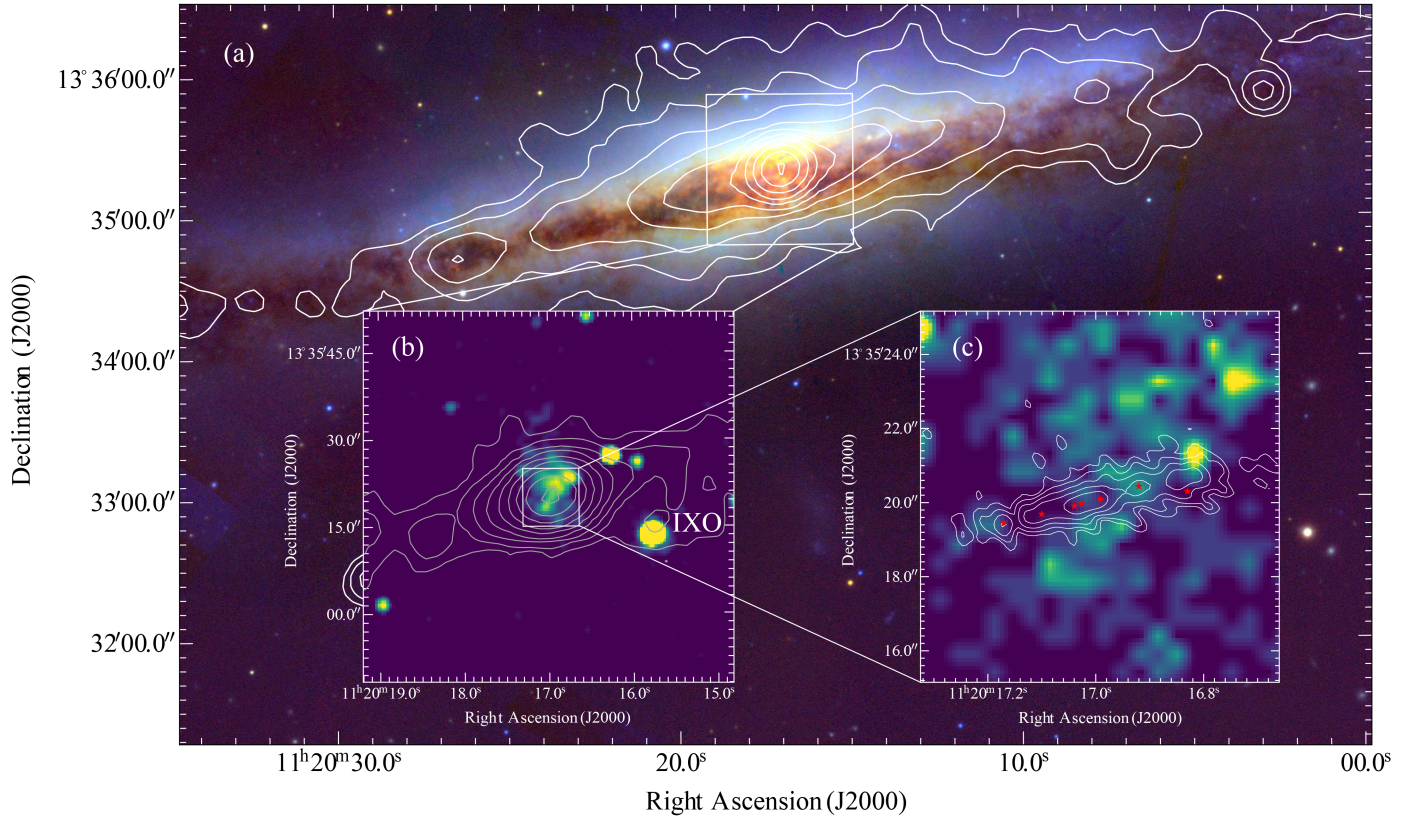


Figure 2. A zooming-in to the central starburst region of NGC 3628. (a) the y , i , g -band color-composite image from Pan-STARRS DR1 (PS1) is overlaid by the VLA D-array 1.5 GHz contours; (b) the FIRST 1.4 GHz contours overlay on the 0.5 – 7 keV *Chandra* X-ray image and the bright point X-ray source is marked as IXO (intermediate-luminosity X-ray object) according to the identification by Strickland et al. (2001); (c) VLA A-array 4.86 GHz radio contours overlay on the *Chandra* X-ray image, where red stars mark the positions of the seven sources detected by VLBA 1.5 GHz (see contours in the middle panel of Figure 1). All the contours are at $3\sigma \times (-1, 1, 2, 4, 8, \dots)$, where 1σ noises are 0.11, 0.15, 0.06 mJy beam $^{-1}$, respectively.

Calibration Database (CALDB)⁷ version 4.9.6 standards using `chandra_repro`. We extracted the X-ray spectrum using the task `specextract`. Previous X-ray observational attention of NGC 3628 is an off-nuclear (20'' from the galaxy center) point X-ray source (see Strickland et al. 2001), other than the diffuse X-ray emissions in the central region of this galaxy. This point X-ray source is bright ($L_{X,0.3,8\text{keV}} = 1.1 \times 10^{40}$ erg s $^{-1}$) and strongly variable, thus belongs to ultraluminous X-ray sources (King et al. 2023) (but it was initially called intermediate-luminosity X-ray object, IXO, by Strickland et al. 2001). In this work, we only concern the nuclear X-ray emissions of this galaxy and we use `specextract` to extract the spectrum of NGC 3628 from a 6''-radius aperture centered on the nuclear X-ray emissions; the background spectrum is extracted from a nearby source-free region. We used photons with energy

ranging from 0.5 to 7.0 keV and grouped the spectrum into 20 photons in each bin.

For cross-checking purposes, we also retrieved the data from *XMM-Newton*. The data was obtained on November 27, 2000 (ObsID: 0110980101, PI: Fred Jansen) with 65 ks. We used the data from all three X-ray detectors: MOS-1, MOS-2, and PN equipped on the European Photon Imaging Cameras (EPIC), and the clean time intervals are 42.2, 42.3, and 32.2 ks, respectively. The EPIC data processing was done with the XMM-Newton Science Analysis System (SAS)⁸ 16.0.0. The tasks `emproc` and `epproc` were used to reprocess the data. To extract the spectrum, we used the same region as with *Chandra* and the energy range of 0.1 and 10 keV. We used the tasks `rmfgen` and `arfgen` to create a response matrix file (RMF) and auxiliary response file (ARF).

⁷ <https://cxc.cfa.harvard.edu/caldb/>

⁸ <https://www.cosmos.esa.int/web/xmm-newton/sas>

Table 1. Radio observational properties of the seven sources in the nuclear region of NGC 3628.

ID	$F_{\text{VLBA},1.5\text{GHz}}$	$d_{\text{VLBA},1.5\text{GHz}}$	$S_{\text{VLBA},1.5\text{GHz}}$	$\theta_{\text{VLBA},1.5\text{GHz}}$	$S_{\text{MERLIN},1.4\text{GHz}}$	$S_{\text{VLA-A},15\text{GHz}}$	$\alpha_{1.4-15\text{GHz}}$	$\log T_{\text{B}}$
	(mJy)	(mas)	(mJy)	(mas)	(mJy)	(mJy)		(K)
(1)	(2)	(3)	(4)	(5)	(6)	(7)	(8)	(9)
C	2.41 ± 0.22	42.2 ± 5.9	2.67 ± 0.21	25.4 ± 1.2	5.7 ± 2.2	2.4 ± 0.2	-0.37 ± 0.21	6.49 ± 0.05
E1	1.67 ± 0.19	36.5 ± 6.7	2.36 ± 0.23	26.3 ± 1.5	7.0 ± 1.1	2.8 ± 0.2	-0.39 ± 0.07	6.41 ± 0.06
E2	0.78 ± 0.12	14.3 ± 3.4	0.81 ± 0.12	8.9 ± 0.8	4.9 ± 1.1	2.3 ± 0.1	-0.32 ± 0.10	5.55 ± 0.11
E3	1.81 ± 0.24	64 ± 14	1.64 ± 0.21	34.2 ± 3.0	2.6 ± 1.1	1.5 ± 0.1	-0.23 ± 0.18	6.02 ± 0.09
E4	1.19 ± 0.16	28.7 ± 6.2	1.21 ± 0.15	16.8 ± 1.4	1.3 ± 1.0	0.4 ± 0.1	-0.50 ± 0.34	6.51 ± 0.09
W1	2.18 ± 0.95	139 ± 84	4.83 ± 3.70	117 ± 33	2.3 ± 0.6	0.8 ± 0.1	-0.45 ± 0.13	5.42 ± 0.41
W2	0.79 ± 0.12	14.2 ± 3.4	0.81 ± 0.12	8.9 ± 0.8	< 0.4	< 0.21	-0.5^\dagger	6.88 ± 0.10

NOTE—Columns give (1) Source ID, (2-3) VLBA 1.5 GHz flux density and diameter with the optically thin sphere model-fit, (4-5) VLBA 1.5 GHz flux density and FWHM of Gaussian model-fit, (6-7) MERLIN 1.4 GHz and VLA 15 GHz flux density, (8) 1.4 (MERLIN) - 15 GHz (VLA) spectral index, and (9) VLBA 1.5 GHz brightness temperature estimated using the parameters from Gaussian model-fit.

NOTE—†: The source was not detected by both MERLIN 1.4 GHz and VLA A-array 15 GHz observations, here we assume a general spectral index for SNRs.

Table 2. Summary of the radio observations of the target NGC 3628.

Telescope	Epoch	Frequency	Bandwidth	θ_{maj}	θ_{min}	PA
		(GHz)	(MHz)	(mas)	(mas)	($^\circ$)
(1)	(2)	(3)	(4)	(5)	(6)	(7)
MERLIN	1996-1	1.4	16	340	300	7.0
MERLIN*	1996-1	1.4	16	260	160	7.0
VLA-A	1986-5	15	100	150	140	-12
VLBA•	2021-7-2	1.5	256	59.5	32.1	46.7
VLBA	2021-7-2	1.5	256	11.2	4.47	-0.63

NOTE—Columns give (1) telescope, (2) observing epoch, (3) frequency, (4) bandwidth, and (5–7) major, minor, and position angle of the beam.

Parameters are estimated under natural weights except for

★: the uniform weight.

●: the uv-taper.

3. RESULTS

In Figure 1, we show VLBA 1.5 GHz images in both high/full (subset images in the top and bottom panels) and low resolution (the middle panel). Based on the VLBA 1.5 GHz observation we identify seven point-like sources under a restoring beam of 59.5×32.1 mas, while two of them (W1 and E2) are too weak and diffuse to be detected in the full-resolution image, and the beam

size of the full-resolution image is 11.2×4.47 mas correspondingly. A two-dimensional Gaussian model-fit is employed to obtain the integrated flux density and the sizes (full width at half maximum of Gaussian models, FWHM) of the compact sources; the model-fitting results are listed in Table 1.

Taking the parameters estimated via Gaussian model-fit for each VLBA source, we can estimate the bright-

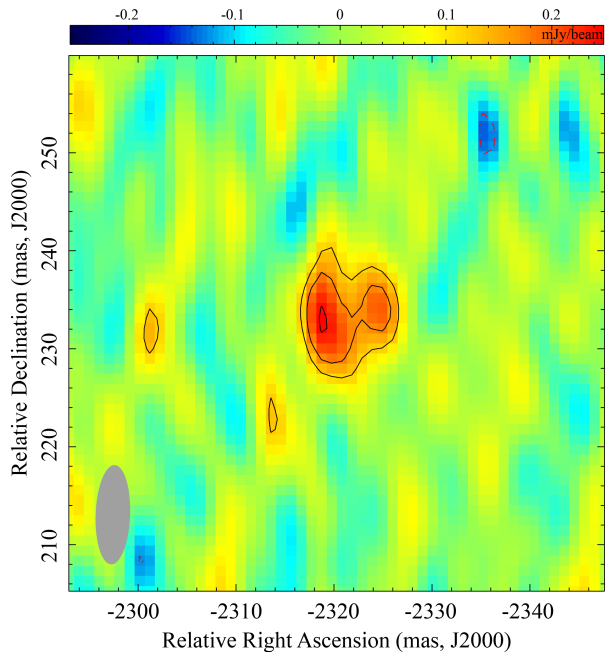


Figure 3. The uniformly weighted VLBA 1.5 GHz image of the source W2. The black solid contours represent positive values and the red dashed contours represent negative values. The contours are at $3\sigma \times (-1, 1, 1.41, 2, 2.83, \dots)$, here 1σ noise is $0.04 \text{ mJy beam}^{-1}$. The grey ellipse in the bottom left corner represents the full width at half-maximum (FWHM) of the restoring beam, it's $10.1 \times 3.51 \text{ mas}$ at -2.07° .

ness temperatures using the formula (e.g. Ulvestad et al. 2005)

$$T_B = 1.8 \times 10^9 (1+z) \frac{S_i}{\nu^2 \theta^2} \text{ (K)}, \quad (1)$$

where S_i is the integrated flux density of each Gaussian model component in mJy (column 2 of Table 1), θ is FWHM of the Gaussian model component in mas (column 6 of Table 1), ν is the observing frequency in GHz, and z is the redshift. The estimated 1.5 GHz brightness temperatures are listed in column 7 of Table 1. Here, the estimated size θ is reliable by comparing it with the full-resolution image of each source. Therefore, it ensues a robust estimation of the radio brightness temperatures. Sources E2 and W1 have the brightness temperatures $\sim 10^5 \text{ K}$, while the others all have brightness temperatures $> 10^6 \text{ K}$ including the highest one W2 (reaching $10^{6.88} \text{ K}$).

We cross-match VLBA and MERLIN sources within 1 beam size (0.26×0.16 at 7.0°) of the MERLIN 1.4 GHz observation (Cole et al. 1998). Six out of the seven VLBA sources (i.e. excepting source W2) have MERLIN counterparts, and VLA A-array 15 GHz sources as well (Carral et al. 1990; Cole et al. 1998), see Table 1. We list the spectral index estimated between MERLIN 1.4 GHz and VLA A-array 15 GHz by Cole et al.

(1998) in column 8 of Table 1. W2 is either a new or a compact (but weak, therefore it is submerged by diffuse foreground radio emissions in previous VLA 15 GHz and MERLIN 1.4 GHz observations) radio source. In Figure 2, we present the optical image of NGC 3628 with radio contours overlaid and the distribution of X-ray emission.

4. DISCUSSION

4.1. Properties of the nuclear radio sources

All the seven radio sources in NGC 3628 have radio brightness temperatures $> 10^5 \text{ K}$, which are thought to have non-thermal origins (Condon 1992). Cole et al. (1998) suggest that six out of the seven radio sources, which have both MERLIN 1.4 GHz and VLA A-array 15 GHz counterparts, are all SNRs based on the spectral indices of -0.23 to -0.50 between 1.4 and 15 GHz. The structures of sources C and E3 may be consistent with partial shells in the full-resolution VLBA images, which further suggests that both of them are SNRs. W2 is the most compact one in our VLBA observation with the highest brightness temperature $\log(T_b/\text{K}) = 6.88$ and the compact structure in the full resolution VLBA image. In addition, we produce a uniformly weighted image of the source W2 (see Figure 3), and it resembles a partial shell of radio SN with asymmetric structure (e.g. Gaensler et al. 1997; Manchester et al. 2005, 2002). Six out of the seven VLBA sources (except W2) distribute along the galaxy disk. Depending on an exponential initial mass function and the fact that most massive stars will become SNe, the linear distribution of the SNe in NGC 3628 hints at an extremely thin, edge-on, and dense inner (~ 250 parsec) star-forming disk. Furthermore, the warping of the galaxy's outer disk is one plausible explanation for the positional discrepancy between W2 and the plane defined by the other six sources and the galaxy.

Based on the transient nature and the partially shell-like morphology, W2 is possibly a radio SN. The lack of an X-ray point source visible in the *Chandra* image makes it less likely that the object is an X-ray binary or an AGN. The non-detection of W2 in both VLA and MERLIN observations in 1986 and 1996, respectively, indicates that either W2 had low radio flux densities at these epochs or it just exploded after 1996. By integrating the Salpeter initial mass function with a power-law slope of $\alpha \approx -2.35$ (see Salpeter 1955; Kroupa 2001; Chabrier 2003; Gunawardhana et al. 2011) and assuming that stars with masses greater than $8 M_\odot$ will eventually become SNe (Heger et al. 2003), the SN rate can be estimated. This calculation results in a 0.2% SN rate trig-

Table 3. Model-fitting results of the X-ray spectra.

Telescope	XSPEC Model	N_{H}	Γ	PL Norm	kT	Mg	Si	Norm ₂	$\chi^2/\text{d.o.f.}$
		(10^{22} cm^{-2})		(10^{-5})	(keV)	(Z_{\odot})	(Z_{\odot})	(10^{-4})	
(1)	(2)	(3)	(4)	(5)	(6)	(7)	(8)	(9)	(10)
<i>Chandra</i>	wabs * powerlaw	0.40 ± 0.07	1.73 ± 0.18	1.46 ± 0.27					39.68/38
<i>Chandra</i>	wabs * (powerlaw + vmekal)	0.71 ± 0.73	1.61 ± 0.38	1.28 ± 0.73	0.27 ± 0.33	9.49 ± 13.2	51.1 ± 76.8	~ 1.71	25.0/38
<i>Chandra</i>	wabs * (powerlaw + vapec)	0.81 ± 0.45	1.64 ± 0.28	1.36 ± 0.55	0.27 ± 0.15	5.35 ± 4.18	29.9 ± 31.2	~ 1.52	23.21/38
<i>XMM-Newton</i>	wabs * powerlaw	0.63 ± 0.13	2.10 ± 0.21	4.31 ± 1.05					16.91/30
<i>XMM-Newton</i>	wabs * (powerlaw + vmekal)	1.26 ± 0.41	2.34 ± 0.25	6.19 ± 2.04	0.45 ± 0.18	~ 0.79	2.03 ± 3.43	1.33 ± 1.94	9.56/30
<i>XMM-Newton</i>	wabs * (powerlaw + vapec)	1.34 ± 0.43	2.27 ± 0.25	5.69 ± 1.94	0.39 ± 0.29	~ 0.14	1.77 ± 2.61	2.32 ± 5.08	9.56/30

NOTE—Columns give (1) telescope, (2) XSPEC models for fit, (3) column density of the neutral Hydrogen, (4–5) photon index and normalization of the power-law model, (6–9) temperature, abundances of the elements Mg and Si, and the normalization of vmekal or vapec model, and (10) fit χ^2 / degrees of freedom.

gered by the star formation rate. The SFR of NGC 3628 is $3.2 M_{\odot} \text{ yr}^{-1}$ (Tsai et al. 2012) or $4.8 M_{\odot} \text{ yr}^{-1}$ (Shinn & Seon 2015), which yields a SN rate of 0.0064 or 0.0096 year^{-1} , respectively. Although these estimates are only approximate, as only a small portion of SNe are radioactive and above the VLBA 1.5 GHz detection limit, it is consistent with the fact that W2 is a nascent SN that has exploded between 2021 (the epoch of VLBA 1.5 GHz observation) and at least 1986.

4.2. The $\Sigma - D$ relation for SNRs

The strength of the synchrotron emissions of the expanding SNRs follows the relation between radio surface brightness Σ and diameter D (the $\Sigma - D$ relation). This relation was initially derived by Shklovskii (1960) via a theoretical deduction and has the form

$$\Sigma_{\nu} = AD^{-\beta}, \quad (2)$$

where parameter A depends on the properties of the SN explosion and surrounding interstellar medium (ISM): the SN energy of the explosion, the mass of ejecta, the density of the ISM, and the strength of the magnetic field, etc., while the slope β is thought to be independent of these properties (Arbutina & Urošević 2005). Subsequent theoretical studies (e.g. Berezhko & Völk 2004; Arbutina & Urošević 2005; Pavlović et al. 2013) show that the $\Sigma - D$ relation is primarily applicable to shell-structure SNRs and obtain the slope β in the range of 2–5.75. Generally, parameters A and β are observationally constrained by fitting the data to a sample of SNRs of known distances (e.g. Urošević et al. 2005; Pavlović et al. 2013; Bozzetto et al. 2017). Establishing a universal $\Sigma - D$ correlation provide a way to study the properties of SNR population in specific galaxies and interstellar environment. Furthermore, Shklovskii (1960) also proposed to use this relation as a method for determining SNR distances.

In order to constrain the parameters in $\Sigma - D$ relation, observations should have a sufficient resolution to measure the diameters of SNRs (they usually maintain a size of sub-parsec to parsec scale, e.g., Fenech et al. 2008; Lenc & Tingay 2009; Batejat et al. 2011; Bondi et al. 2012; Rampadarath et al. 2014) in star-forming galaxies. Based on the SN/SNR nature of the seven sources in NGC 3628, we fit the optically thin sphere model to the uv-data for each source to obtain integrated flux density and size. Firstly, we perform the model fit on the full-resolution image to get the models of sources C, E1, E3, E4, and W2; then model the sources W1 and E2 on the uv-tapered data. The results are listed in columns 2 and 3 of Table 1. It can be found that the flux densities from the optically thin sphere model-fit (column 2 of Table 1) are consistent with those from the Gaussian model-fit (column 4 of Table 1), while the diameters of sphere models (column 3 of Table 1) are systematically larger than the FWHM of Gaussian models (column 5 of Table 1). This can be identified by marking these two sizes on the full-resolution images of each component (top and bottom panels of Figure 1). Obviously, the diameter of the sphere model indicates the outer boundary, while the FWHM of the Gaussian model indicates the size of the brightest emitting features. The optically thin sphere model is retrieved based on the identification of these sources as SNRs, and therefore it is more applicable to representing the source sizes.

We can fit the empirical $\Sigma - D$ correlation by establishing a well-resolvable SNR sample. In this work, we involve SNRs that are detected in several nearby galaxies (Urošević et al. 2005; Filipović et al. 2005; Fenech et al. 2008; Chomiuk & Wilcots 2009; Bozzetto et al. 2017), however, we decide to not use the SNR sample from Arp220 due to the poor resolutions (Batejat et al. 2011). For SNRs in nearby low-redshift galaxies, we estimate 1 GHz surface brightness

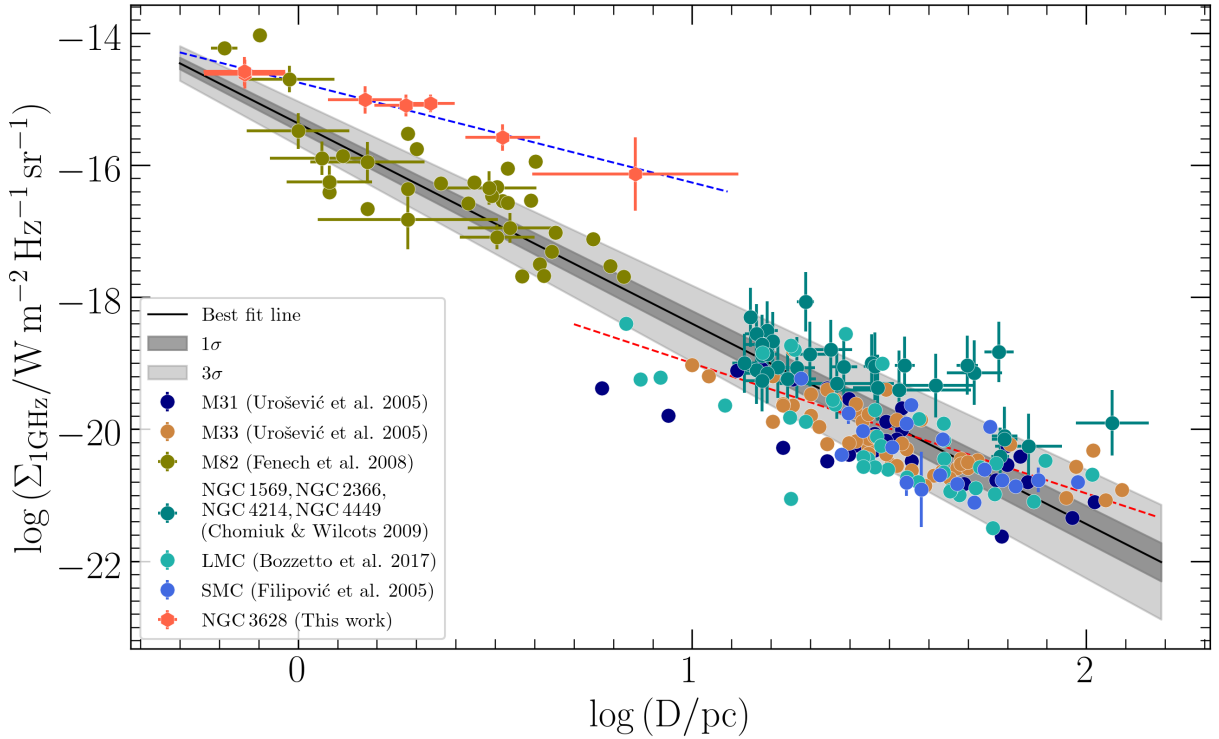


Figure 4. The 1 GHz surface brightness versus diameter relation for SNRs. The solid black line represents the best fit of the full SNR samples and the grey belts are 1σ and 3σ intervals. The blue- and red-dashed lines are the best fits for the SNR sample in NGC 3628 and in local galaxies except for M82 and NGC 3628, respectively.

$\Sigma_{1\text{GHz}}$ ($\text{W m}^{-2} \text{Hz}^{-1} \text{sr}^{-1}$) through the formula

$$\Sigma_{1\text{GHz}} = 5.417 \times 10^{-16} \frac{S_{1\text{GHz}}}{\theta^2(1+z)^{(1+\alpha)}}, \quad (3)$$

where $S_{1\text{GHz}}$ is the integrated 1 GHz flux density in Jansky (Jy), θ is the diameter in arcsecond, α is the spectral index. The radio surface brightness doesn't depend on the distance to the SNRs. Our VLBA data has been extrapolated to 1 GHz by using the spectral index in column 8 of Table 1.

Figure 4 shows the surface brightness distribution along the diameters of SNRs, obviously, the SNRs which are detected in NGC 3628 follow the trend of the full sample. We fit a power law to the full SNR samples and get the correlation

$$\Sigma_{1\text{GHz}} = (4.23 \pm 1.07) \times 10^{-16} D^{-3.03 \pm 0.08}. \quad (4)$$

This fit shows a good regression and obtains the correlation slope $\beta = 3.03 \pm 0.08$, which is slightly flatter than the fit by Bozzetto et al. (2017), i.e. $\beta = 3.60 \pm 0.15$. This slight difference is due to the use of the new SNR sample of NGC 3628 in this work and the removal of the SNRs in Arp220 for fit. Fitting the SNR sample in NGC 3628 gives a power-law slope $\beta = 1.51 \pm 0.12$. This slope is comparable with the value $\beta = 1.97 \pm 0.16$ obtained for SNRs in the local galaxy samples except for

M82 and NGC 3628. The slope for SNRs in NGC 3628 is consistent with that in M31 and M33 ($\beta = 1.67$ and $\beta = 1.77$, respectively Urošević et al. 2005), and NGC 1569 ($\beta = 1.26 \pm 0.2$, Sánchez-Cruces et al. 2022). It should be noted that the slope $\beta \approx 2$ is generally a statistical rather than a physical cause (Arbutina & Urošević 2005; Sánchez-Cruces et al. 2022). However, the positive correlation between the surface brightness of SNRs and the ISM density, and the type of SNRs would naturally result in an individual $\Sigma - D$ relation for each extragalactic SNR sample. Furthermore, a high-resolution radio observation is important to measure the sizes of each SNR and constrain the $\Sigma - D$ relation.

4.3. Origin of the nuclear diffuse X-ray emission

We extract *Chandra* X-ray spectrum directly from the central $12''$ region, which includes both diffuse and point-like X-ray sources (see Figure 2). In starburst galaxies, point X-ray emission may originate from X-ray binaries (e.g. Long et al. 2014) or AGNs (e.g. Komossa et al. 2003). Therefore, we firstly fitted an absorbed power law model to the *Chandra* spectrum (the green line in Figure 5 and the parameters are listed in Table 3), which follows the overall trend of the data in the count rate versus energy plot. Interestingly, by subtracting the continuum emission (the power law), we

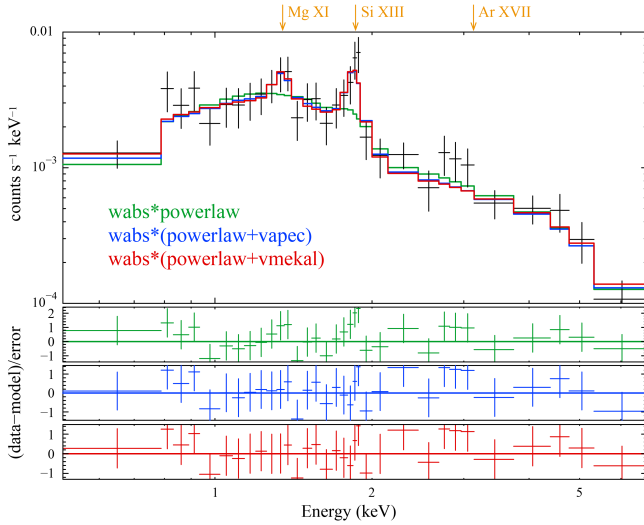


Figure 5. *Chandra* spectrum and model-fits. The solid lines show the best-fitting models to the data in the energy range 0.5–7 keV, and each lower panel shows the corresponding residuals. Models from the top to the bottom panels are `wabs*powerlaw`, `wabs*(powerlaw+vapec)`, `wabs*(powerlaw+vmekal)`, respectively.

see several narrow features which overlap with the emission lines Mg XI and Si XIII (the rest-frame energies are 1.331 and 1.839 keV, respectively), and possibly Ar XVII (3.104 keV) and a combination of O VII (spans 0.653 to 0.654 keV), Fe XVII (spans 0.725 to 0.739 keV) and Ne IX (spans 0.905 to 0.922 keV) lines. These lines are abundant in SNRs and are clear features of their X-ray spectra (e.g. Holt et al. 1994; Hughes et al. 2000; Michael et al. 2002; Badenes et al. 2006; Badenes 2010; Saito et al. 2020).

Therefore, we added a thermal plasma component to model the *Chandra* and *XMM-Newton* spectra. Two plasma models are individually added to the spectral fitting: collisional ionization equilibrium gas (`apec` model in XSPEC) and hot diffuse MeKal gas (`vmekal` model in XSPEC). In the spectral fitting, we only fit the abundances of the elements O, Fe, Ne, Mg, Si, and Ar, and fix the abundances of the other elements. However, we can only constrain the abundances (in units of solar abundance Z_{\odot}) of the elements Mg and Si (see Table 3), which indicate a supersolar abundance. These two models well represent the X-ray spectra along with the line features, which give better χ_{red}^2 of 0.65 and 0.61 for models `wabs*(powerlaw+vmekal)` and `wabs*(powerlaw+vapec)` for the *Chandra* spectrum, respectively. The over-fitting indicated by the χ_{red}^2 is likely due to the limited number of data points.

Here the power-law component accounts for the possible contributions from XRBs and AGNs. Given that

the radio emission of NGC 3628 is dominated by star-forming activity, we can explore the correlation between X-ray and radio luminosity for NGC 3628. This correlation is regulated by the fact that both the radio and X-ray emissions are from star-forming activities, especially the X-ray emissions, are dominated by XRBs. We use a comparison sample of 43 star-forming galaxies with detection in both radio and X-ray bands from Vattakunnel et al. (2012). A strong correlation was found in the comparison sample between the hard X-ray luminosity $\log L_{X,2-10\text{keV}}$ in erg s^{-1} and 1.4 GHz flux density $\log L_{1.4\text{GHz}}$ in W Hz^{-1} .

$$\log L_{X,2-10\text{keV}} = (1.04 \pm 0.05) \log L_{1.4\text{GHz}} + (17.68 \pm 1.15), \quad (5)$$

and the slope is very close to unity for local star-forming galaxies. Furthermore, we fit the correlation between the soft X-ray luminosity $\log L_{X,0.5-2\text{keV}}$ in W Hz^{-1} and 1.4 GHz flux density for the comparison sample and find a correlation

$$\log L_{X,0.5-2\text{keV}} = (0.89 \pm 0.06) \log L_{1.4\text{GHz}} + (20.71 \pm 1.47). \quad (6)$$

We use the correlations here to estimate soft and hard X-ray luminosities for NGC 3628 and we take the FIRST 1.4 GHz luminosity $\log(L_{1.4\text{GHz}}/\text{W Hz}^{-1}) = 21.58$, where the emission region constrained through FIRST observation well overlaps with that through *Chandra* (see panel b of Figure 2). The resulting $\log(L_{X,0.5-2\text{keV}}/\text{erg s}^{-1}) = 39.91 \pm 1.95$ and $\log(L_{X,2-10\text{keV}}/\text{erg s}^{-1}) = 40.12 \pm 1.57$, which are ~ 1.32 and ~ 1.08 -dex higher than the intrinsic soft $\log(L_{X,0.5-2\text{keV}}/\text{erg s}^{-1}) = 38.58 \pm 0.01$ and hard X-ray luminosity $\log(L_{X,2-10\text{keV}}/\text{erg s}^{-1}) = 39.03 \pm 0.05$ of NGC 3628, respectively, though with high uncertainties.

Furthermore, we employ the non-linear L_X –SFR correlation derived by Grimm et al. (2003)

$$\text{SFR} (M_{\odot} \text{ yr}^{-1}) = \left(\frac{L_{X,2-10\text{keV}}}{2.6 \times 10^{39} \text{ erg s}^{-1}} \right)^{0.6}, \quad (7)$$

to estimate the X-ray emissions produced by star-forming activities. This non-linear correlation only works for low SFR galaxies (e.g. Mineo et al. 2014). Taking the SFR = $3.2 M_{\odot} \text{ yr}^{-1}$ (or SFR = $4.8 M_{\odot} \text{ yr}^{-1}$, see Shinn & Seon 2015) estimated from IR luminosity (Tsai et al. 2012), the X-ray luminosity of NGC 3628 is calculated as $\log(L_{X,2-10\text{keV}}/\text{erg s}^{-1}) = 40.25$, while the *Chandra* observations obtain a intrinsic (i.e. unabsorbed) X-ray luminosity $\log(L_{X,2-10\text{keV}}/\text{erg s}^{-1}) = 39.03 \pm 0.05$. The estimated 2–10 keV X-ray luminosity via the above equation is ~ 1.22 -dex higher than

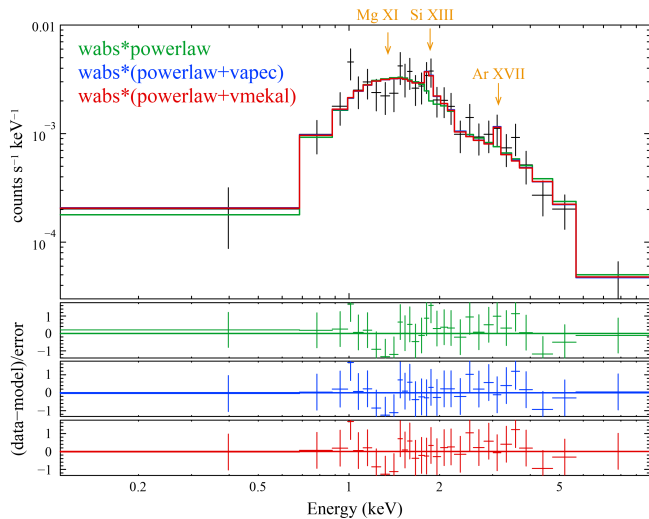


Figure 6. *XMM-Newton* 0.1 – 10 keV spectrum of NGC 3628 and model-fits. The green, blue, and red lines represent the best fits with the model `wabs*powerlaw`, `wabs*(powerlaw+vapec)`, `wabs*(powerlaw+vmekal)`, respectively. The corresponding residuals of the best fits are shown in the bottom panel.

Table 4. Model-fitting parameters for *Chandra* 0.5 – 7 keV spectrum with XSPEC module `wabs*(vrnei+vmekal)`.

Model component	Parameter	Value
wabs	N_{H} ($\times 10^{22}$ cm $^{-2}$)	0.68 ± 0.44
	Norm. ($\times 10^5$)	2.32 ± 7.13
	kT (keV)	1.46 ± 0.27
vrnei	kT_{init} (keV)	0.31 ± 0.63
	τ ($\times 10^{13}$ cm $^{-3}$ s)	> 4.53
	Mg (Z_{\odot})	6.11 ± 5.12
	Si (Z_{\odot})	28.6 ± 28.4
	Norm. ($\times 10^5$)	4.35 ± 0.68
vmekal	kT (keV)	10.1 ± 11.4
	Mg (Z_{\odot})	≤ 9.67
	Si (Z_{\odot})	≤ 4.61

NOTE—Parameters are: N_{H} , the column density of the neutral Hydrogen; kT , the electron temperature; kT_{init} , the initial plasma temperature; τ , the ionization timescale; and the abundances of each element.

the observations. Taking the recent $L_{\text{X}} - \text{SFR}$ correlation derived by Bayliss et al. (2020) still results in an overestimation of X-ray luminosity.

These results imply insufficient XRBs in the central region of the galaxy NGC 3628, and they disfavor an AGN

as well. Indeed, the high resolution ($\sim 0.5''$) *Chandra* observation shows that the X-ray emission neither overlaps with the radio emissions (see panel c of Figure 2) nor associates with the individual radio source (e.g. the cases of X-ray SNe/SNRs, Long et al. 2014). Furthermore, the X-ray emission has a symmetric morphology extending in both the north and south of the galaxy disk, which mimics a galactic scale wind (see also Tsai et al. 2012). Interestingly, the *Chandra* spectrum presented in this work (including both diffuse and point-like X-ray emission) is highly consistent with the point-source subtracted spectrum (see Tsai et al. 2012), which again implies a deficit of point X-ray sources.

Therefore, we account for the X-ray emissions from activities that are triggered by SNRs. We modeled the *Chandra* spectra with a combination of a thermal gas (`vmekal` model in XSPEC) and a nonequilibrium ionization plasma (`vrnei` model in XSPEC), which correspond to the interstellar medium and the ejecta of SNRs (see Saito et al. 2020), respectively. The abundance of elements O, Fe, Ne, Mg, Si, and Ar are free parameters, while the others are fixed to the solar abundance. The best-fit parameters and spectral lines are presented in Table 4 and Figure 7, respectively. The fitting yields electron temperatures of 1.46 ± 0.27 keV and 10.1 ± 11.4 keV for NEI and MeKaL medium, respectively. Interestingly, the fit not only represents the emission lines Mg XI and Si XIII, but also the lines Ar XVII at 3.104 keV and the combination of O VIII, Fe XVII, and Ne IX lines at 0.7–0.8 keV. The abundances of Mg and Si are roughly consistent with the `wabs*(powerlaw+vapec)` and `wabs*(powerlaw+vmekal)`. Obviously, this model better represents the spectrum and the associated narrow features than the above models, though it has an over-fitting $\chi_{\text{red}}^2 = 0.62$ due to the limited data points. As a result, this model indicates that the X-ray emissions in the central region of NGC 3628 can be fully explained by SN-triggered activities. Along with the morphology of the X-ray emitting regions, the X-ray emissions trace a hot and highly ionized galactic scale gas outflow of NGC 3628.

5. CONCLUSION

We conducted a study on the radio and X-ray emissions of the starburst galaxy NGC 3628, and have summarized our findings as follows. (1) Through the VLBA 1.5 GHz observation, we achieved the highest resolution of $\sim 5\text{--}10$ mas and were able to resolve the central dominating radio sources of this galaxy. This ensues the identification of seven compact SNRs in galaxy NGC 3628, and three of them are consistent with partial shells; (2) We estimated the diameter of these seven sources by fit-

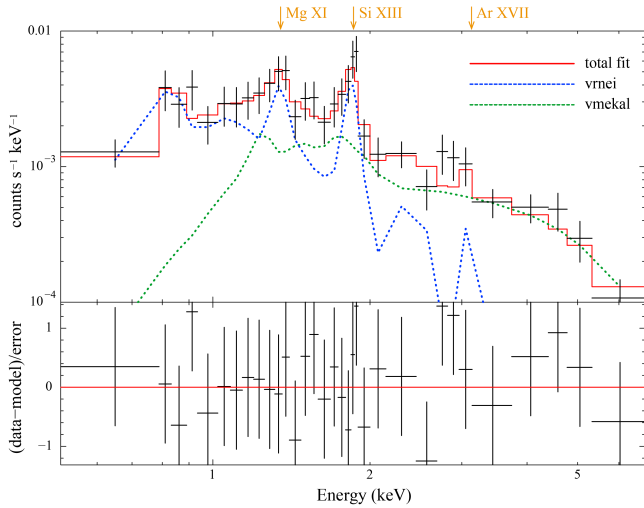


Figure 7. *Chandra* 0.5–7 keV X-ray spectrum of NGC 3628. The red solid line corresponds to the best-fitting model $\mathbf{wabs*(vrnei+vmekal)}$, where the \mathbf{vrnei} model shows in blue dashed line and the \mathbf{vmekal} model shows in green dashed line. The residuals of the best fit are shown in the bottom panel.

ting an optically thin sphere model, and we discovered that one of these seven sources is a new radio SN; (3) We explored the $\Sigma - D$ relation by using the SNRs detected in NGC 3628 and other SNR samples with accurate size estimations; (4) We analyzed archival observations of NGC 3628 from *Chandra* and *XMM-Newton* with a total effective exposure time of more than 170 ks. We found that the X-ray spectra can be well modeled with the activities of SNRs; (5) We investigated the correlation between X-ray luminosity and star-formation rate, as well as the correlation between radio and X-ray luminosity for starburst galaxies. Our findings suggest that the X-ray emission is more likely to originate from the activities of SNRs than from X-ray binaries and AGNs. These results indicate that SN-triggered activities are responsible for producing both X-ray and radio emissions in the starburst galaxy NGC 3628. This work provides valuable insights into the SN-driven radio activity and galactic-scale gas outflow model.

This research was supported by the National Key R&D Program of China (Grant No. 2020YFE0202100), the Shanghai Sailing Program (21YF1455300), the National Science Foundation of China (12103076), and the China Postdoctoral Science Foundation (2021M693267). Scientific results from the data presented in this publication are derived from the VLBA Project BA146. The National Radio Astronomy Observatory is a facility of the National Science Foundation operated under cooperative agreement by Associated Universities, Inc.

REFERENCES

- Arbutina, B., & Urošević, D. 2005, *MNRAS*, 360, 76, doi: [10.1111/j.1365-2966.2005.09033.x](https://doi.org/10.1111/j.1365-2966.2005.09033.x)
- Badenes, C. 2010, *Proceedings of the National Academy of Science*, 107, 7141, doi: [10.1073/pnas.0914189107](https://doi.org/10.1073/pnas.0914189107)
- Badenes, C., Borkowski, K. J., Hughes, J. P., Hwang, U., & Bravo, E. 2006, *ApJ*, 645, 1373, doi: [10.1086/504399](https://doi.org/10.1086/504399)
- Baskin, A., & Laor, A. 2021, *MNRAS*, 508, 680, doi: [10.1093/mnras/stab2555](https://doi.org/10.1093/mnras/stab2555)
- Batejat, F., Conway, J. E., Hurley, R., et al. 2011, *ApJ*, 740, 95, doi: [10.1088/0004-637X/740/2/95](https://doi.org/10.1088/0004-637X/740/2/95)
- Bayliss, M. B., McDonald, M., Sharon, K., et al. 2020, *Nature Astronomy*, 4, 159, doi: [10.1038/s41550-019-0888-7](https://doi.org/10.1038/s41550-019-0888-7)
- Becker, R. H., White, R. L., & Helfand, D. J. 1995, *ApJ*, 450, 559, doi: [10.1086/176166](https://doi.org/10.1086/176166)
- Berezhko, E. G., & Völk, H. J. 2004, *A&A*, 427, 525, doi: [10.1051/0004-6361:20041111](https://doi.org/10.1051/0004-6361:20041111)
- Beswick, R. J., Riley, J. D., Marti-Vidal, I., et al. 2006, *MNRAS*, 369, 1221, doi: [10.1111/j.1365-2966.2006.10363.x](https://doi.org/10.1111/j.1365-2966.2006.10363.x)
- Bondi, M., Pérez-Torres, M. A., Herrero-Illana, R., & Alberdi, A. 2012, *A&A*, 539, A134, doi: [10.1051/0004-6361/201118446](https://doi.org/10.1051/0004-6361/201118446)
- Bozzetto, L. M., Filipović, M. D., Vukotić, B., et al. 2017, *ApJS*, 230, 2, doi: [10.3847/1538-4365/aa653c](https://doi.org/10.3847/1538-4365/aa653c)
- Carral, P., Turner, J. L., & Ho, P. T. P. 1990, *ApJ*, 362, 434, doi: [10.1086/169280](https://doi.org/10.1086/169280)
- Chabrier, G. 2003, *PASP*, 115, 763, doi: [10.1086/376392](https://doi.org/10.1086/376392)
- Chevalier, R. A., & Clegg, A. W. 1985, *Nature*, 317, 44, doi: [10.1038/317044a0](https://doi.org/10.1038/317044a0)
- Chomiuk, L., & Wilcots, E. M. 2009, *AJ*, 137, 3869, doi: [10.1088/0004-6256/137/4/3869](https://doi.org/10.1088/0004-6256/137/4/3869)
- Cicone, C., Maiolino, R., Sturm, E., et al. 2014, *A&A*, 562, A21, doi: [10.1051/0004-6361/201322464](https://doi.org/10.1051/0004-6361/201322464)
- Cole, G. H. J., Mundell, C. G., & Pedlar, A. 1998, *MNRAS*, 300, 656, doi: [10.1046/j.1365-8711.1998.01870.x](https://doi.org/10.1046/j.1365-8711.1998.01870.x)
- Combes, F. 2000, in *Astronomical Society of the Pacific Conference Series*, Vol. 197, *Dynamics of Galaxies: from the Early Universe to the Present*, ed. F. Combes, G. A. Mamon, & V. Charmandaris, 15. <https://arxiv.org/abs/astro-ph/9908145>
- Condon, J. J. 1992, *ARA&A*, 30, 575, doi: [10.1146/annurev.aa.30.090192.003043](https://doi.org/10.1146/annurev.aa.30.090192.003043)
- Cooper, J. L., Bicknell, G. V., Sutherland, R. S., & Bland-Hawthorn, J. 2008, *ApJ*, 674, 157, doi: [10.1086/524918](https://doi.org/10.1086/524918)
- Di Matteo, P., Combes, F., Melchior, A. L., & Semelin, B. 2007, *A&A*, 468, 61, doi: [10.1051/0004-6361:20066959](https://doi.org/10.1051/0004-6361:20066959)
- Engelbracht, C. W., Rieke, M. J., Rieke, G. H., Kelly, D. M., & Achtermann, J. M. 1998, *ApJ*, 505, 639, doi: [10.1086/306176](https://doi.org/10.1086/306176)
- Fall, S. M., Krumholz, M. R., & Matzner, C. D. 2010, *ApJL*, 710, L142, doi: [10.1088/2041-8205/710/2/L142](https://doi.org/10.1088/2041-8205/710/2/L142)
- Falstad, N., Aalto, S., König, S., et al. 2021, *A&A*, 649, A105, doi: [10.1051/0004-6361/202039291](https://doi.org/10.1051/0004-6361/202039291)
- Fenech, D., Beswick, R., Muxlow, T. W. B., Pedlar, A., & Argo, M. K. 2010, *MNRAS*, 408, 607, doi: [10.1111/j.1365-2966.2010.17144.x](https://doi.org/10.1111/j.1365-2966.2010.17144.x)
- Fenech, D. M., Muxlow, T. W. B., Beswick, R. J., Pedlar, A., & Argo, M. K. 2008, *MNRAS*, 391, 1384, doi: [10.1111/j.1365-2966.2008.13986.x](https://doi.org/10.1111/j.1365-2966.2008.13986.x)
- Filipović, M. D., Payne, J. L., Reid, W., et al. 2005, *MNRAS*, 364, 217, doi: [10.1111/j.1365-2966.2005.09554.x](https://doi.org/10.1111/j.1365-2966.2005.09554.x)
- Fomalont, E. B. 1999, in *Astronomical Society of the Pacific Conference Series*, Vol. 180, *Synthesis Imaging in Radio Astronomy II*, ed. G. B. Taylor, C. L. Carilli, & R. A. Perley, 301
- Fruscione, A., McDowell, J. C., Allen, G. E., et al. 2006, in *Society of Photo-Optical Instrumentation Engineers (SPIE) Conference Series*, Vol. 6270, *Society of Photo-Optical Instrumentation Engineers (SPIE) Conference Series*, ed. D. R. Silva & R. E. Doxsey, 62701V, doi: [10.1117/12.671760](https://doi.org/10.1117/12.671760)
- Gaensler, B. M., Manchester, R. N., Staveley-Smith, L., et al. 1997, *ApJ*, 479, 845, doi: [10.1086/303917](https://doi.org/10.1086/303917)
- Gallimore, J. F., Baum, S. A., & O'Dea, C. P. 2004, *ApJ*, 613, 794, doi: [10.1086/423167](https://doi.org/10.1086/423167)
- Gerke, J. R., Kochanek, C. S., & Stanek, K. Z. 2015, *MNRAS*, 450, 3289, doi: [10.1093/mnras/stv776](https://doi.org/10.1093/mnras/stv776)
- Greisen, E. W. 2003, in *Astrophysics and Space Science Library*, Vol. 285, *Information Handling in Astronomy - Historical Vistas*, ed. A. Heck, 109, doi: [10.1007/0-306-48080-8_7](https://doi.org/10.1007/0-306-48080-8_7)
- Grimm, H. J., Gilfanov, M., & Sunyaev, R. 2003, *MNRAS*, 339, 793, doi: [10.1046/j.1365-8711.2003.06224.x](https://doi.org/10.1046/j.1365-8711.2003.06224.x)
- Gunawardhana, M. L. P., Hopkins, A. M., Sharp, R. G., et al. 2011, *MNRAS*, 415, 1647, doi: [10.1111/j.1365-2966.2011.18800.x](https://doi.org/10.1111/j.1365-2966.2011.18800.x)
- Heckman, T. M., Armus, L., & Miley, G. K. 1990, *ApJS*, 74, 833, doi: [10.1086/191522](https://doi.org/10.1086/191522)
- Heger, A., Fryer, C. L., Woosley, S. E., Langer, N., & Hartmann, D. H. 2003, *ApJ*, 591, 288, doi: [10.1086/375341](https://doi.org/10.1086/375341)
- Hermosa Muñoz, L., Márquez, I., Cazzoli, S., Masegosa, J., & Agís-González, B. 2022, *A&A*, 660, A133, doi: [10.1051/0004-6361/202142629](https://doi.org/10.1051/0004-6361/202142629)

- Holt, S. S., Gotthelf, E. V., Tsunemi, H., & Negoro, H. 1994, *PASJ*, 46, L151
- Hopkins, P. F., Hernquist, L., Cox, T. J., et al. 2006, *ApJS*, 163, 1, doi: [10.1086/499298](https://doi.org/10.1086/499298)
- Hughes, J. P., Rakowski, C. E., Burrows, D. N., & Slane, P. O. 2000, *ApJL*, 528, L109, doi: [10.1086/312438](https://doi.org/10.1086/312438)
- Inoue, Y., & Doi, A. 2018, *ApJ*, 869, 114, doi: [10.3847/1538-4357/aaeb95](https://doi.org/10.3847/1538-4357/aaeb95)
- Irwin, J. A., & Sofue, Y. 1996, *ApJ*, 464, 738, doi: [10.1086/177360](https://doi.org/10.1086/177360)
- Johnson, K. E., Kobulnicky, H. A., Massey, P., & Conti, P. S. 2001, *ApJ*, 559, 864, doi: [10.1086/322335](https://doi.org/10.1086/322335)
- King, A., Lasota, J.-P., & Middleton, M. 2023, *NewAR*, 96, 101672, doi: [10.1016/j.newar.2022.101672](https://doi.org/10.1016/j.newar.2022.101672)
- Kobulnicky, H. A., & Johnson, K. E. 1999, *ApJ*, 527, 154, doi: [10.1086/308075](https://doi.org/10.1086/308075)
- Komossa, S., Burwitz, V., Hasinger, G., et al. 2003, *ApJL*, 582, L15, doi: [10.1086/346145](https://doi.org/10.1086/346145)
- Kroupa, P. 2001, *MNRAS*, 322, 231, doi: [10.1046/j.1365-8711.2001.04022.x](https://doi.org/10.1046/j.1365-8711.2001.04022.x)
- Laor, A., & Behar, E. 2008, *MNRAS*, 390, 847, doi: [10.1111/j.1365-2966.2008.13806.x](https://doi.org/10.1111/j.1365-2966.2008.13806.x)
- Lehnert, M. D., & Heckman, T. M. 1996, *ApJ*, 472, 546, doi: [10.1086/178086](https://doi.org/10.1086/178086)
- Lenc, E., & Tingay, S. J. 2009, *AJ*, 137, 537, doi: [10.1088/0004-6256/137/1/537](https://doi.org/10.1088/0004-6256/137/1/537)
- Long, K. S., Kuntz, K. D., Blair, W. P., et al. 2014, *ApJS*, 212, 21, doi: [10.1088/0067-0049/212/2/21](https://doi.org/10.1088/0067-0049/212/2/21)
- Lonsdale, C. J., Diamond, P. J., Thrall, H., Smith, H. E., & Lonsdale, C. J. 2006, *ApJ*, 647, 185, doi: [10.1086/505193](https://doi.org/10.1086/505193)
- Manchester, R. N., Gaensler, B. M., Staveley-Smith, L., Kesteven, M. J., & Tzioumis, A. K. 2005, *ApJL*, 628, L131, doi: [10.1086/432836](https://doi.org/10.1086/432836)
- Manchester, R. N., Gaensler, B. M., Wheaton, V. C., et al. 2002, *PASA*, 19, 207, doi: [10.1071/AS01042](https://doi.org/10.1071/AS01042)
- Marcaide, J. M., Alberdi, A., Ros, E., et al. 1995, *Science*, 270, 1475, doi: [10.1126/science.270.5241.1475](https://doi.org/10.1126/science.270.5241.1475)
- Marcaide, J. M., Martí-Vidal, I., Alberdi, A., et al. 2009, *A&A*, 505, 927, doi: [10.1051/0004-6361/200912133](https://doi.org/10.1051/0004-6361/200912133)
- McCray, R., & Kafatos, M. 1987, *ApJ*, 317, 190, doi: [10.1086/165267](https://doi.org/10.1086/165267)
- McQuinn, K. B. W., Skillman, E. D., Heilman, T. N., Mitchell, N. P., & Kelley, T. 2018, *MNRAS*, 477, 3164, doi: [10.1093/mnras/sty839](https://doi.org/10.1093/mnras/sty839)
- Michael, E., Zhekov, S., McCray, R., et al. 2002, *ApJ*, 574, 166, doi: [10.1086/340591](https://doi.org/10.1086/340591)
- Middelberg, E., Agudo, I., Roy, A. L., & Krichbaum, T. P. 2007, *MNRAS*, 377, 731, doi: [10.1111/j.1365-2966.2007.11639.x](https://doi.org/10.1111/j.1365-2966.2007.11639.x)
- Mihos, J. C., & Hernquist, L. 1996, *ApJ*, 464, 641, doi: [10.1086/177353](https://doi.org/10.1086/177353)
- Mineo, S., Gilfanov, M., Lehmer, B. D., Morrison, G. E., & Sunyaev, R. 2014, *MNRAS*, 437, 1698, doi: [10.1093/mnras/stt1999](https://doi.org/10.1093/mnras/stt1999)
- Montuori, M., Di Matteo, P., Lehnert, M. D., Combes, F., & Semelin, B. 2010, *A&A*, 518, A56, doi: [10.1051/0004-6361/201014304](https://doi.org/10.1051/0004-6361/201014304)
- Neff, S. G., Ulvestad, J. S., & Teng, S. H. 2004, *ApJ*, 611, 186, doi: [10.1086/383608](https://doi.org/10.1086/383608)
- Nims, J., Quataert, E., & Faucher-Giguère, C.-A. 2015, *MNRAS*, 447, 3612, doi: [10.1093/mnras/stu2648](https://doi.org/10.1093/mnras/stu2648)
- Pannuti, T. G., Swartz, D. A., Laine, S., et al. 2015, *AJ*, 150, 91, doi: [10.1088/0004-6256/150/3/91](https://doi.org/10.1088/0004-6256/150/3/91)
- Parra, R., Conway, J. E., Diamond, P. J., et al. 2007, *ApJ*, 659, 314, doi: [10.1086/511813](https://doi.org/10.1086/511813)
- Pavlović, M. Z., Urošević, D., Vukotić, B., Arbutina, B., & Göker, Ü. D. 2013, *ApJS*, 204, 4, doi: [10.1088/0067-0049/204/1/4](https://doi.org/10.1088/0067-0049/204/1/4)
- Pedlar, A., Muxlow, T. W. B., Garrett, M. A., et al. 1999, *MNRAS*, 307, 761, doi: [10.1046/j.1365-8711.1999.02642.x](https://doi.org/10.1046/j.1365-8711.1999.02642.x)
- Pradel, N., Charlot, P., & Lestrade, J. F. 2006, *A&A*, 452, 1099, doi: [10.1051/0004-6361:20053021](https://doi.org/10.1051/0004-6361:20053021)
- Raginski, I., & Laor, A. 2016, *MNRAS*, 459, 2082, doi: [10.1093/mnras/stw772](https://doi.org/10.1093/mnras/stw772)
- Rampadarath, H., Morgan, J. S., Lenc, E., & Tingay, S. J. 2014, *AJ*, 147, 5, doi: [10.1088/0004-6256/147/1/5](https://doi.org/10.1088/0004-6256/147/1/5)
- Rinaldi, P., Caputi, K. I., van Mierlo, S. E., et al. 2022, *ApJ*, 930, 128, doi: [10.3847/1538-4357/ac5d39](https://doi.org/10.3847/1538-4357/ac5d39)
- Rioja, M. J., Dodson, R., Orosz, G., Imai, H., & Frey, S. 2017, *AJ*, 153, 105, doi: [10.3847/1538-3881/153/3/105](https://doi.org/10.3847/1538-3881/153/3/105)
- Rovilos, E., Diamond, P. J., Lonsdale, C. J., Smith, H. E., & Lonsdale, C. J. 2005, *MNRAS*, 359, 827, doi: [10.1111/j.1365-2966.2005.08853.x](https://doi.org/10.1111/j.1365-2966.2005.08853.x)
- Roy, A., Nath, B. B., Sharma, P., & Shchekinov, Y. 2016, *MNRAS*, 463, 2296, doi: [10.1093/mnras/stw2127](https://doi.org/10.1093/mnras/stw2127)
- Saito, M., Yamauchi, S., Nobukawa, K. K., Bamba, A., & Pannuti, T. G. 2020, *PASJ*, 72, 65, doi: [10.1093/pasj/psaa042](https://doi.org/10.1093/pasj/psaa042)
- Salpeter, E. E. 1955, *ApJ*, 121, 161, doi: [10.1086/145971](https://doi.org/10.1086/145971)
- Sánchez-Cruces, M., Sardaneta, M. M., Fuentes-Carrera, I., et al. 2022, *MNRAS*, 513, 1755, doi: [10.1093/mnras/stac985](https://doi.org/10.1093/mnras/stac985)
- Schweizer, F. 2005, in *Astrophysics and Space Science Library*, Vol. 329, *Starbursts: From 30 Doradus to Lyman Break Galaxies*, ed. R. de Grijs & R. M. González Delgado, 143, doi: [10.1007/1-4020-3539-X_25](https://doi.org/10.1007/1-4020-3539-X_25)
- Sharp, R. G., & Bland-Hawthorn, J. 2010, *ApJ*, 711, 818, doi: [10.1088/0004-637X/711/2/818](https://doi.org/10.1088/0004-637X/711/2/818)

- Shepherd, M. C. 1997, in *Astronomical Society of the Pacific Conference Series*, Vol. 125, *Astronomical Data Analysis Software and Systems VI*, ed. G. Hunt & H. Payne, 77
- Shetty, R., & Ostriker, E. C. 2008, *ApJ*, 684, 978, doi: [10.1086/590383](https://doi.org/10.1086/590383)
- Shinn, J.-H., & Seon, K.-I. 2015, *ApJ*, 815, 133, doi: [10.1088/0004-637X/815/2/133](https://doi.org/10.1088/0004-637X/815/2/133)
- Shklovskii, I. S. 1960, *Soviet Ast.*, 4, 243
- Skinner, M. A., & Ostriker, E. C. 2015, *ApJ*, 809, 187, doi: [10.1088/0004-637X/809/2/187](https://doi.org/10.1088/0004-637X/809/2/187)
- Strickland, D. K., Colbert, E. J. M., Heckman, T. M., et al. 2001, *ApJ*, 560, 707, doi: [10.1086/323055](https://doi.org/10.1086/323055)
- Strickland, D. K., Heckman, T. M., Colbert, E. J. M., Hoopes, C. G., & Weaver, K. A. 2004, *ApJS*, 151, 193, doi: [10.1086/382214](https://doi.org/10.1086/382214)
- Strickland, D. K., Heckman, T. M., Weaver, K. A., Hoopes, C. G., & Dahlem, M. 2002, *ApJ*, 568, 689, doi: [10.1086/338889](https://doi.org/10.1086/338889)
- Tomisaka, K., & Ikeuchi, S. 1988, *ApJ*, 330, 695, doi: [10.1086/166505](https://doi.org/10.1086/166505)
- Tsai, A.-L., Matsushita, S., Kong, A. K. H., Matsumoto, H., & Kohno, K. 2012, *ApJ*, 752, 38, doi: [10.1088/0004-637X/752/1/38](https://doi.org/10.1088/0004-637X/752/1/38)
- Ulvestad, J. S. 2009, *AJ*, 138, 1529, doi: [10.1088/0004-6256/138/5/1529](https://doi.org/10.1088/0004-6256/138/5/1529)
- Ulvestad, J. S., Antonucci, R. R. J., & Barvainis, R. 2005, *ApJ*, 621, 123, doi: [10.1086/427426](https://doi.org/10.1086/427426)
- Urošević, D., Pannuti, T. G., Duric, N., & Theodorou, A. 2005, *A&A*, 435, 437, doi: [10.1051/0004-6361:20042535](https://doi.org/10.1051/0004-6361:20042535)
- Varenius, E., Conway, J. E., Batejat, F., et al. 2019, *A&A*, 623, A173, doi: [10.1051/0004-6361/201730631](https://doi.org/10.1051/0004-6361/201730631)
- Vattakunnel, S., Tozzi, P., Matteucci, F., et al. 2012, *MNRAS*, 420, 2190, doi: [10.1111/j.1365-2966.2011.20185.x](https://doi.org/10.1111/j.1365-2966.2011.20185.x)
- Wehrle, A. 1987, in *Bulletin of the American Astronomical Society*, Vol. 19, 718
- Wik, D. R., Lehmer, B. D., Hornschemeier, A. E., et al. 2014, *ApJ*, 797, 79, doi: [10.1088/0004-637X/797/2/79](https://doi.org/10.1088/0004-637X/797/2/79)
- Yang, J., Yang, X., Wrobel, J. M., et al. 2022a, *MNRAS*, 514, 6215, doi: [10.1093/mnras/stac1753](https://doi.org/10.1093/mnras/stac1753)
- Yang, X., Mohan, P., Yang, J., et al. 2022b, arXiv e-prints, arXiv:2211.00050. <https://arxiv.org/abs/2211.00050>
- Yang, X., Wang, R., & Guo, Q. 2022c, *MNRAS*, 517, 4959, doi: [10.1093/mnras/stac2990](https://doi.org/10.1093/mnras/stac2990)
- Yang, X., Yao, S., Yang, J., et al. 2020, *ApJ*, 904, 200, doi: [10.3847/1538-4357/abb775](https://doi.org/10.3847/1538-4357/abb775)
- Zakamska, N. L., & Greene, J. E. 2014, *MNRAS*, 442, 784, doi: [10.1093/mnras/stu842](https://doi.org/10.1093/mnras/stu842)
- Zhang, Z.-Y., Romano, D., Ivison, R. J., Papadopoulos, P. P., & Matteucci, F. 2018, *Nature*, 558, 260, doi: [10.1038/s41586-018-0196-x](https://doi.org/10.1038/s41586-018-0196-x)